Rendiconti Lincei. Scienze Fisiche e Naturali (2024) 35:25–36
https://doi.org/10.1007/s12210-023-01215-8

Scattering of diatomic molecules from graphite

Maria Rutigliano[1] · **Fernando Pirani**[2,3]

Received: 20 October 2023 / Accepted: 12 December 2023 / Published online: 16 January 2024

Abstract
In the last years, state-to-state molecular dynamics simulations of some basic elementary processes, occurring at the gas–surface interface in a wide range of temperatures and collision energies, have been performed by adopting new potential energy surfaces. In this contribution, our attention is mostly addressed to the role of long-range forces, determining the physisorption of gaseous molecules on the surface. Such forces, formulated in terms of the improved Lennard–Jones interaction potential model, control the formation of precursor or pre-reactive state that plays a crucial role in the dynamical evolution of molecules impinging on the surface in the range of low–intermediate collision kinetic energies. The study focuses on the collisions of H_2, O_2, N_2 and CO, initially in their ground and excited vibro-rotational levels, on a graphite surface. The resulting dispersion coefficients, which control the capture of impinging molecules, are compared and found in good agreement with those available in the literature. New selectivity and peculiarities of scattered molecules, crucial to control the kinetics of elementary chemical processes occurring at the gas–surface interfaces under thermal and sub-thermal conditions, of interest in different applied fields, are highlighted.

Keywords Molecular dynamics simulations · Potential energy surface · Long-range interactions · Inelastic scattering · Graphite · Energetics

1 Introduction

Elastic, inelastic and reactive collision events, driven by intermolecular forces and occurring at the gas–surface inter-phases, are of interest for the control of the dynamical evolution of elementary processes of interest in several fields, including reactivity, chemical kinetics, plasmas physics and chemistry, catalysis and energy reservoirs. Moreover, the interaction of atoms/molecules with cold surfaces is also strictly related to astronomical observations. In fact, molecular collisions represent excellent probes of chemical–physics conditions in interstellar medium (IM) controlled by quantities such as pressure, density and temperature, typically ranging over low values. Furthermore, atoms/molecules, driven by non-covalent interaction components, on dust grains, whose temperature is lower than 100 K, give rise mainly to physisorption with adsorption energy around 100 meV. Grains act as catalysts for the formation or deactivation of molecules. The hydrogen molecule case represents a paradigmatic example of this statement. Indeed, H_2: (1) is the precursor of more complex molecules; (2) is dissociated by cosmic rays and UV radiation; (3) is abundant in IM and in particular a high ratio of H_2/H is observed in dense clouds. For many years it has been supposed that H_2 is produced on the surface of cold carbonaceous grains to explain these concomitant observations.

Starting from a basic previous work (Rutigliano et al. 2001), in the last 20 years, many experimental and

This peer-reviewed research paper is part of the Topical Collection originated from contributions to the conference on "Chemical Kinetics at Micro-, Meso-, Bioscales", dedicated to Giangualberto Volpi (1928–2017, Linceo from 1994),organized by Accademia Nazionale dei Lincei and Fondazione Guido Donegani in Rome, March 27–28, 2023.

✉ Maria Rutigliano
maria.rutigliano@cnr.it

Fernando Pirani
pirani.fernando@gmail.com

[1] CNR-ISTP (Istituto per la Scienza e Tecnologia dei Plasmi), Via Amendola 122/D, 70126 Bari, Italy

[2] Dipartimento di Chimica, Biologia e Biotecnologie, Università di Perugia, Via Elce di Sotto 8, 06123 Perugia, Italy

[3] Dipartimento di Ingegneria Civile ed Ambientale, Università di Perugia, Via G. Duranti 93, 06125 Perugia, Italy

theoretical studies have been performed by different groups on this subject, with different methods and, then, at different degrees of accuracy (see for example Greighan et al. 2006; Kristensen et al. 2011; Casolo et al. 2013; Wakelam et al. 2017, and references therein). Note again that collisions at low energy and involving ground-state molecules with cold surfaces are of great interest for sub-thermal phenomena, as those occurring in cold environments of IM (Agúndez and Wakelam 2013).

In addition, molecule–surface collisions under thermal and hyper-thermal conditions are of interest for controlling chemical kinetics in plasmas and for heterogeneous catalysis. In particular, molecular plasmas are of interest for different applications ranging from environment (Lea et al. 2020) to aerospace (Rutigliano and Pirani 2019), passing from thermonuclear fusion (Cartry et al. 2012) and plasma-assisted catalysis (Hanna et al 2019).

Among the different elementary processes storing energy in molecular vibro-rotational states, those promoted by collisions at the gas–surface interface certainly play a primary role. In fact, chemi-/physisorption of molecules can lead to their dissociation as well as to their elastic and/or inelastic backscattering in the gas phase. The dynamics of elementary processes involved directly controls the energy exchange mechanisms between the surface and the internal degrees of freedom of incident molecules. Furthermore, molecular dissociation at the surface produces atoms and/or free radicals that, if trapped on the surface, modify its chemical and thermal properties, or if diffused into the gas phase, they can act as very effective collision quenchers (Cacciatore and Rutigliano 2009). All these elementary processes are of crucial relevance for a modelling as realistic as possible of complex phenomena occurring in the various applied fields listed above.

In light of these considerations, in the last years, we studied the interaction between prototype diatomic molecules as $H_2(v_i, j_i)$, $O_2(v_i, j_i)$, $N_2(v_i, j_i)$ and $CO(v_i, j_i)$ with graphite, where v_i and j_i are the number defining, respectively, the initial vibrational and rotational state of impinging molecules (Rutigliano and Pirani 2016, 2018, 2019, 2020a, 2021). Such molecules have been assumed in several initial roto-vibrational states. The effects of these interactions on the gas–surface collision events have been characterized by performing molecular dynamics (MD) simulations, in a wide collision energy range investigating, in some cases, the role of the surface temperature (Ts). Our MD study involved three different steps: (I) building of a 3D crystal lattice of graphite for which we determined the phonons dynamics; (II) determination of new potential energy surfaces (PES) driving the fate of gas–surface collision events. In particular, for the part relating to the chemisorption, we used results derived from density functional theory (DFT) calculations. In contrast, for that relating to long-range interactions, where the failure of the DFT is well known, we used the improved Lennard–Jones (ILJ) potential formulation (Pirani et al. 2008); (III) propagation and analysis of tens of thousands of trajectories, in the framework of a semiclassical collisional method (Billing 2000) to cast light on the reaction dynamics. Therefore, from the analysis of trajectories, we can determine the collisional data, such as probabilities of elementary surface processes and roto-vibrational distributions of the final products that can be used to characterize the reaction kinetics of the system under study for the considered application.

Therefore, this paper aims to provide additional information on the strength of the weak non-covalent gas–surface interactions and on the selectivity of the scattering processes occurring from sub-thermal up to thermal collision energy (E_{coll}) range, where the precursor state formed by the trapping of gaseous molecules on the surface plays a basic role. Specifically, E_{coll} is assumed to change from 0.001 up to 0.1 eV, that is in the interval: 10^{-4} up to 10 kJ/mol, while potential wells associated with the physisorption state vary from tens up to hundreds of meV (from a few up to tens kJ/mol).

Here, we will give a roundup of the main results obtained in the investigation of the scattering of H_2, O_2, N_2 and CO, in their ground and excited roto-vibrational levels, from a graphite surface for collision kinetic energies and surface temperatures of interest for several phenomena (see above) occurring under thermal and sub-thermal conditions. In particular, some previously obtained information is combined with new results and, in several cases, the use of the same conditions allows a proper comparison of the results obtained for the different impinging molecules.

The next section reports on new features of the interaction controlling the physisorption states formation with a detailed comparison of the strength of the long-range attraction. A quick overview of our MD calculation method is given in Sect. 3, whilst some dynamical results and discussion on the main predicted peculiarities are reported in Sect. 4. Finally, in Sect. 5 general conclusions are set out.

2 Physisorption states

The formation of the precursor state, affecting the kinetics of elementary processes, whose stability and selectivity are controlled by the long-range attraction, as that arising from dispersion forces, will be properly emphasized in this section. Table 1 reports the values of the leading C_6 dispersion coefficient, associated with the long-range attraction contribution from each pair formed by the gaseous particle-effective atom of the surface. The same table provides the C_3 coefficient, defining the global attraction of the gaseous particle from the entire surface.

Table 1 Values of C_6 and C_3 long-range attraction coefficients. The obtained C_3 values are compared, when available, with the results reported in the literature (Vidali et al. 1991)

Interacting pair	C_6 (meVÅ^6)	C_3 (meVÅ^3) our results	C_3 (meVÅ^3) literature
He–Gr	3113	185	180 ± 15
Ne–Gr	6786	402	346
Ar–Gr	22584	1339	1210
Kr–Gr	33454	1985	1730
Xe–Gr	49913	2961	2460
H–Gr	6385	379	380 ± 17
H_2–Gr	9016	535	520 ± 30
N–Gr	13505	801	
N_2–Gr	22658	1344	1259
O–Gr	10319	612	
O_2–Gr	20446	1213	1157
C–Gr	17554	1041	
CO–Gr	23227	1378	
CH_4–Gr	31525	1870	1746

All given values refer to atom/molecule interacting with graphite. They have been extracted from the ILJ formulation of the interaction (Rutigliano and Pirani 2016, 2019, 2020a, 2021) or semiempirically predicted by a phenomenological method (Cambi et al 1991). Note that the following equation (Israelachvili 1991) relates the two different long-range coefficients:

$$C_3 = \frac{\pi C_6 n}{6}, \tag{1}$$

where n is the density of the atoms in the surface, which for graphite amounts to 0.1133 atoms/Å^3.

Data reported in Table 1 suggest some important comments: (i) the systems involving noble gas atoms and the polyatomic CH_4, for which accurate C_3 values obtained with different methods are available from the literature (Vidali et al. 1991), have been used as test of our approach; (ii) our results, derived from the asymptotic behaviour of the ILJ function or semiempirically predicted, have been substantially obtained in an internally consistent way that is within the same methodology, for all systems; (iii) the comparison indicates that both (present and literature) reported long-range coefficients approximately scale with the polarizability of the gaseous species (Werner and Meyer 1976; Olney et al. 1997), while their absolute values depends also on effective polarizability of the atoms of the surface and on their density; (iv) the dependence of the C_3 on the polarizability of the gaseous species, interacting with the same surface (graphite), is displayed in Fig. 1; (v) it is important also to note that in our approach the

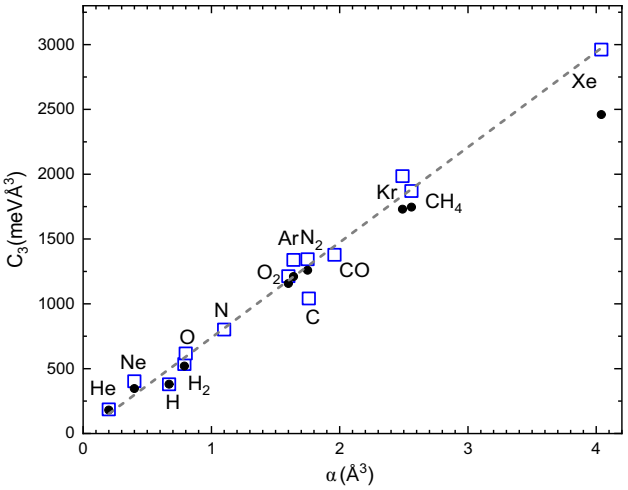

Fig. 1 C_3 coefficients calculated for rare gases, nitrogen (atomic and molecular), oxygen (atomic and molecular), and carbon monoxide (molecule and atoms formed for molecular dissociation) as a function of polarizability (α) of the gaseous species (Werner and Meyer 1976 for atoms; Olney et al. 1997 for molecules), interacting with graphite (blue open squares) are compared with the data from literature (Vidali et al. 1991) (black full dots). Uncertainty on the polarizability of noble gas atoms and molecules is of the order of 1÷2 percent, that on H polarizability is zero, since obtainable by "exact" quantum mechanical treatments, and that of C, N and O atoms is at most 6÷7 percent. For the C atoms forming the graphite, we have chosen α = 1.3 Å^3, a value different with respect to that (α = 1.76 Å^3) of isolated C in the gas phase. The line reproducing the linear fit according to Eq. (2) is also reported (grey dashed line)

possible role of many body effects is probably enclosed in the choice of the effective polarizability of atoms forming the surface, whose value is different with respect that of the gaseous atoms, because their valence electrons are involved in the formation of chemical bonds with neighbouring atoms, defining the structure and stability of the surface. Figure 1 also emphasizes some small deviations from the linearity that we attribute to the role of the different number of polarizable-outher electrons when passing from a gaseous species to another (Cambi et al. 1991). For instance, H–Gr and C–Gr systems provide a well-evident deviation. In particular, H shows a polarizability value (0.67 Å^3) higher with respect to that of Ne (0.40 Å^3), but the C_3 coefficients for H–Gr and Ne–Gr assume comparable magnitude, since in the case of Ne the effective number of polarizable-outher electrons is much higher (about a factor 7) with respect to H. It has been demonstrated (Cambi et al. 1991) that increasing the number of polarizable-outher electrons of an interacting partner also the dispersion attraction increases since the probability of electronic cloud deformation changes by contributing to the induced dipole formation. Another interesting case is C–Gr compared with N_2–Gr: gaseous C and N_2 exhibit the same polarizability value, but the

number of effective electrons for C is about one-half of that for N_2.

Despite the small deviations from the linearity found, we carried out a linear fit of the calculated data according to which obtained C_3 values for the interaction of different species on graphite can be described by the following relationship corresponding to the dashed line of Fig. 1.

$$C_3 = A + B * \alpha \tag{2}$$

with $A = 4.023 \text{meV}\text{Å}^3$ and $B = 735.00$ meV.

Therefore, given the good agreement with the data available in the literature, obtained with different methods, we can deduce that the interaction of any interacting species with graphite can be calculated by Eq. (2), the polarizability known.

The adopted approach has proven worthy for the determination of C_3 coefficients with an error of the order of $10\% \div 15\%$, which is comparable to or slightly larger than the uncertainty associated with each value from the literature. In addition, it predicts results more in line with the data reported in the literature with respect to the values obtained in the framework of the DFT with long-range corrections. Indeed, for the typical physisorption process of Ar atom adsorption on graphite, a value for C_3 of 2057 $\text{meV}\text{Å}^3$ is reported in (Ambrosetti and Silvestrelli 2012) by using DFT/vdW-WF2 that results much higher than both the value reported in Vidali et al. (1991) and the one here determined (see Table 1).

3 Molecular dynamics simulations

MD simulations, carried out exploiting a computational setup based on a state-to-state semiclassical collision method (Billing 2000), have been successfully used in the last 40 years for the description of basic gas–surface processes. The method is described in detail in several publications and in particular in Billing's book (Billing 2000). We like to remark here that the method provides detailed knowledge of the single-/multi-phonon inelastic processes that assist the dynamics of the surface processes due to the chemi- and physisorption of atoms and molecules on different substrates. This is, indeed, the most important peculiarity of our semiclassical approach. According to this method, the dynamics of the gas-phase species impinging the surface is described classically, whereas the dynamics of surface phonons is obtained by solving the time-dependent Schrödinger equations of motion for a set of (3*N*-6) independent harmonic oscillators, with *N* being the total number of atoms in the lattice, perturbed by the external forces exerted between the impinging species and the surface. The dynamical coupling between the surface atom vibrations and the translational motion of gas-phase particle is obtained by solving the classical Hamilton's equations for the following Hamiltonian:

$$H = \frac{1}{2}\sum_i \frac{P_i^2}{m_i} + V(r) + \Delta E_{ph} + V_{eff}\left(t, T_S\right), \tag{3}$$

where P_i is the momentum of atom i having mass m_i in the molecule, $V(r)$ is the intramolecular interaction potential and $V_{\text{eff}}(t, T_S)$ is the effective potential of mean field type, depending on time and surface temperature and ΔE_{ph} is the total energy exchanged between the impinging molecule and the phonons. The latter is obtained as the sum of the energy due to the phonon creation/annihilation processes (Billing 2000) (Rutigliano and Pirani 2022 2023).

As stressed in the Introduction section, such a method exploits a sequence of different operational steps, involving the determination of the 3D surface model structure and the corresponding surface phonon dynamics, the building of the PES driving the gas–surface process under study, and the propagation of a sufficiently large number of classical trajectories in the adopted framework. For major details see for instance Rutigliano and Pirani (2016, 2019, 2020a, 2021, 2022, 2023).

The considered graphite surface model assumed in the MD simulations consists of 186 atoms and the density of phonons states used here is that reported in Rutigliano and Cacciatore (2008). The PES for the intermolecular interaction of H_2, O_2, N_2, and CO with graphite has been obtained as the sum of pairwise atom–atom interactions between the single atom in the impinging molecule and C atoms in the graphite lattice (Rutigliano and Pirani 2016, 2019, 2020a, 2021).

In the simulations, we set the initial conditions with respect to a Cartesian frame of reference centred on the surface plane and having the *Z*-axis normal to the surface pointing out towards the vacuum. The (*X*–*Y*) plane lies on the surface top layer. In the simulation, molecules are initially placed at a distance $Z = 10$ Å sufficiently far from the surface to correspond to the asymptotic free region. They approach the clean graphite surface in the normal direction to the surface plane ($\theta = 0°$), while the azimuthal angle is chosen randomly at the beginning of each trajectory. The collision energy ranged between 0.001 and up to 2.0 eV and T_S between 10 and 800 K depending on the application interest for the considered molecule–graphite interaction. The initial position coordinates (*X*, *Y*) are chosen randomly on the considered surface.

In the trajectory analysis, we can distinguish different surface processes including molecular scattering, molecule adsorption dissociation, molecule dissociation with the scattering of two resulting atoms, and adsorption/

desorption in which one atom remains on the surface and the other is scattered in gas phase.

4 Results and discussion

In the present study, the simulated collision stereodynamics indicates that after the interaction with the graphite surface, molecules are backscattered mainly in a direction very close to the specular one. Moreover, while v_i is usually preserved in all investigated cases, the final rotational states, j_f, of O_2, N_2 and CO, exhibit non-Boltzmann distributions with the main peak nearby $j_f = j_i$ and a secondary maximum at high j_f. The hydrogen molecule is a case in itself because of its peculiar rotational state sequence/separation. In particular, when H_2 molecules impinge in $j_i = 0$, the final rotational distribution has a maximum in $j_f = 1$, while for $j_i > 0$ the final distribution has a peak in $j_f = j_i$.

These and other features of rotational distributions also suggest a close correlation between the initial rotational configuration of impinging molecules and the final state achieved after the scattering (Rutigliano and Pirani 2019, 2020a, 2021). These findings, complementary to those from molecular beam (MB) experiments (for the cases of O_2 and N_2 see Vattuone et al. 2010 and references therein), cast light on relevant selectivity of elastic and inelastic collision events that control the stereodynamics of several elementary processes occurring both in gaseous and condensed phases for low energy (as those met in the interstellar medium) as well as for higher energy as those of interest for aerospace applications.

However, for comparing rotational distributions, it should be proper to consider the different separation of levels of investigated molecules, thus discussing them in terms of the value of the energy corresponding to the maximum of distribution, rather than of the level.

Accordingly, in the present study, we assumed the different diatomic molecules in the same initial rotovibrational state $j_i = 1$, $v_i = 0$, impinging on the graphite surface, taken at $T_S = 100$ K, at two different collision energy values. Therefore, we compared the final rotational distributions in terms of the corresponding level energies

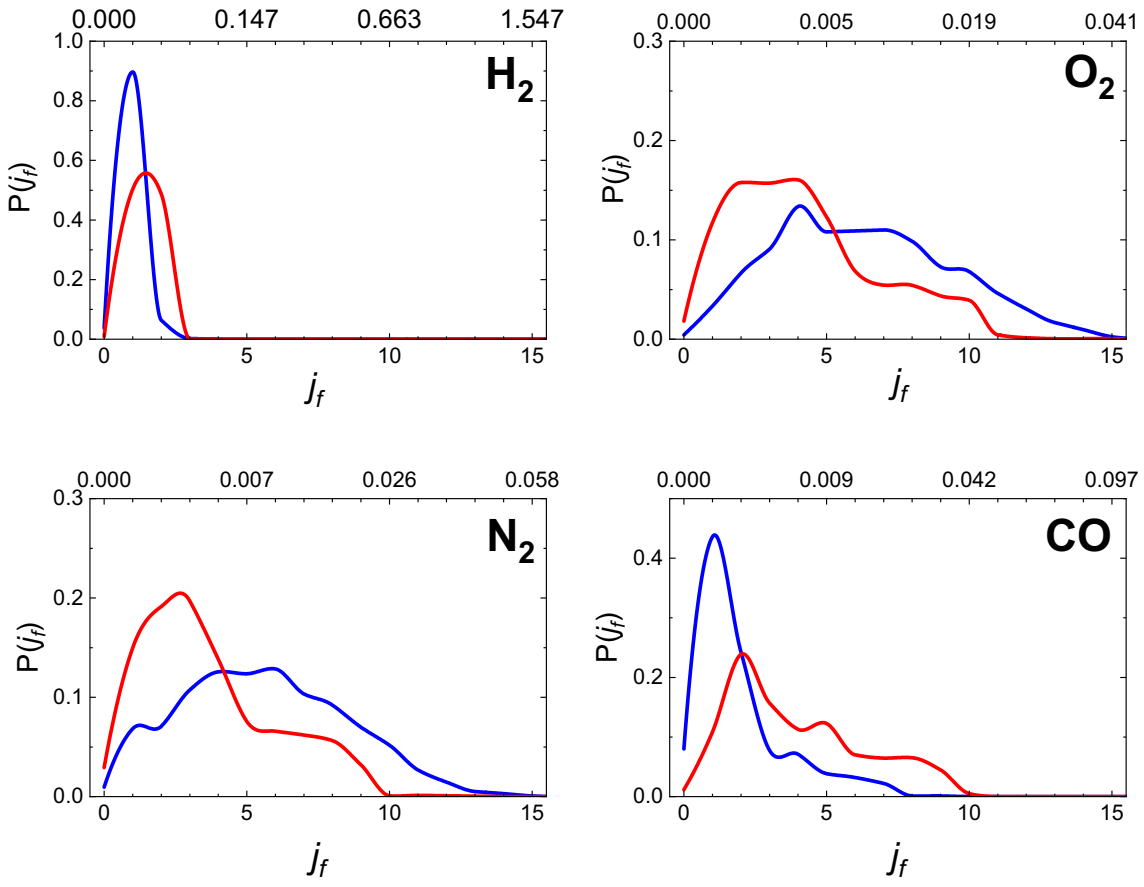

Fig. 2 Comparison of final rotational distributions for H_2, O_2, N_2, and CO molecules initially in (0, 1) scattered by the graphite surface for $E_{coll} = 0.01$ eV (blue line) and $E_{coll} = 0.1$ eV (red line). The rotational energies, again given in eV, corresponding to the rotational levels indicated on the bottom *X*-axis, are reported for easy comparison on the top *X*-axis. In the simulations, $T_S = 100$ K is assumed

and the obtained results are shown in Fig. 2. It emerges that the energy corresponding to the maximum, as expected, is inversely proportional to the molecule mass and, therefore, the rotational energy of the main peak of distribution decreases starting from H_2 and ending with O_2. Moreover, for the lowest E_{coll} value, H_2 and CO rotational distributions exhibit a sharp peak that, increasing the collision energy, remains only for H_2.

MD simulations have highlighted the coupling between translational and rotational motion of molecules approaching the surface. In particular, both the fate of trajectories and final rotational distributions are the direct result of such coupling, although, mainly for the lower collision energies, the energy arising from the coupling with the surface phonons also contributes to the reaction dynamics. However, the effect of long-range interactions and, therefore, of physisorption is more evident for low collision energies, that is when E_{coll} becomes comparable to the interaction energy involved in the adsorption process.

Further specific peculiarities, obtained for the inelastic scattering of hydrogen, oxygen, nitrogen, and carbon monoxide molecules impinging on graphite in well-defined initial roto-vibrational states and at selected E_{coll}, will be presented and discussed separately in the following subsections.

4.1 Hydrogen

Present MD simulations confirm that when an $H_2(v_i, j_i)$ molecule impinges on the graphite surface, even at very low E_{coll}, it is reflected in the gas phase following a direct mechanism, in the sense that the molecule is immediately scattered after the interaction with the surface, and preserving its initial vibrational state. Under such conditions, the reaction dynamics is mostly controlled by rotational excitation that determines the fate of each trajectory.

Figure 3 reports the probability of the first four final rotational states (j_f) formation as a function of E_{coll} for molecules impinging the graphite surface in two different initial vibrational ($v_i = 0,1$) states, but in the same initial rotational level ($j_i = 1$). From such a figure, it appears that except for $j_f = 0$ and in the region of very low collision energy, the probability for the other values of j_f is the same, irrespective of considered v_i and E_{coll} values.

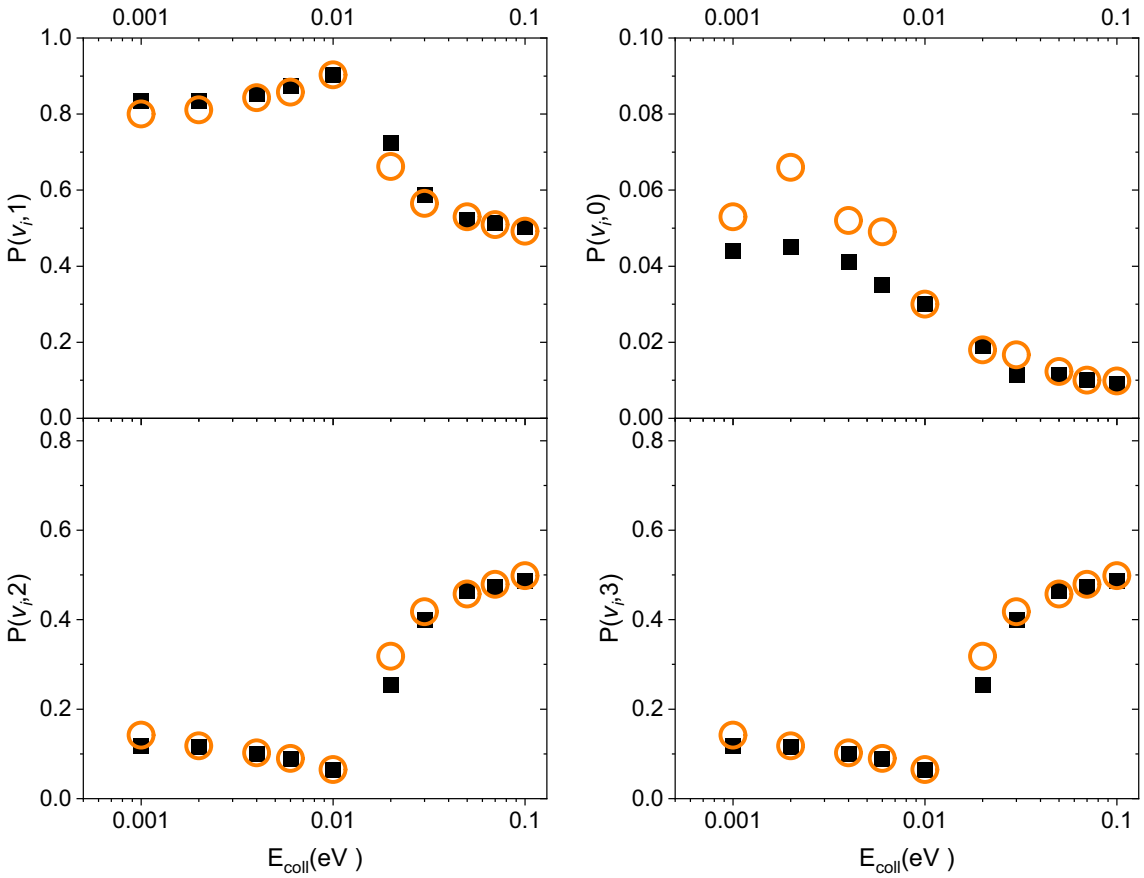

Fig. 3 (Partially adapted from Fig. 7 of Rutigliano and Pirani 2016). Final rotational distributions for $H_2(v_i,1)$. The cases of $v_i = 0$ (orange circles) and $v_i = 1$ (black squares) are considered

Moreover, MD simulations did not highlight any surface temperature effect when the same bunches of trajectories have been propagated for different T_S values. The interested reader can refer to Rutigliano and Pirani (2016) for the complete set of results concerning the scattering of $H_2(v_i, j_i)$ from a graphite surface, while results for its isotopologue molecules can be found in(Rutigliano and Pirani (2018).

4.2 Oxygen

Capturing O_2 by the graphite surface is more efficient than H_2 since the long-range dispersion attraction is at least a factor 2 stronger (see Table 1) and the physisorption potential well is significantly deeper. Therefore, in the case of the interaction of $O_2(v_i, j_i)$ with a graphite surface, it is found that for the ground vibrational state and collision energies of $E_{coll} = 0.01$ eV and $E_{coll} = 0.1$ eV, an appreciable percentage of trajectories end with sticking. This feature appears in Fig. 4, where the probability for scattering and sticking for three different values of j_i is reported. From such a figure it also emerges that the sticking, for a given E_{coll} value, decreases as j_i increases, helping the rotating molecule to escape from the physisorption potential well.

For oxygen molecules, the reaction mechanism can be direct, as emphasized for hydrogen, or indirect in the sense that the molecule remains trapped close to the surface for a while, bouncing many times, before being reflected in the gas phase. For low collision energy, the initial vibrational level is preserved for low v_i values, while molecules in high initial vibrational levels are scattered vibrationally excited. Moreover, for high collision energy values, molecules can be scattered either excited or deactivated vibrationally. Surface

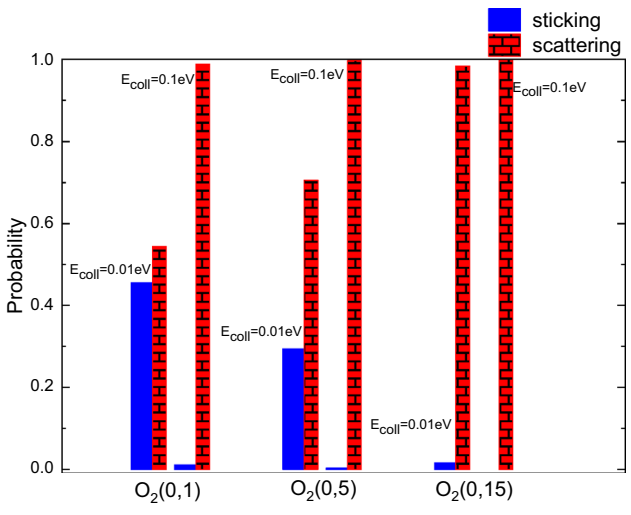

Fig. 4 (Partially adapted from Fig. 2 of Rutigliano and Pirani 2020b). Surface processes probability for oxygen molecule in $v_i = 0$ and $j_i = 1$, 5, 15

temperature effects become appreciable only at very low collision energy, when interaction potential energies at the play are comparable with those of surface phonons (Rutigliano and Pirani 2019).

A very accurate trajectory analysis revealed the important selectivity with regard to the excitation/de-excitation of rotational levels, controlled by the orientation of the molecular rotation axis (or rotation plane) of projectiles with respect to the target, here the surface, and already observed in MB experiments probing molecular collisions in the gas phase (Aquilanti et al. 1999). In fact, molecules approaching the surface with a *cartwheel*-type motion undergo a pronounced rotation excitation and are backscattered with $j_f > j_i$. On the other end, molecules moving with *helicopter*-type motion are elastically backscattered with $j_f \approx j_i$ (Rutigliano and Pirani 2019).

An example of trajectory (1D and 3D), associated with the scattering occurring at medium–low collision energy and leading to a remarkable final rotational excitation, together with rotational state and energetic terms evolution, is shown in Fig. 5 to give further light on this fundamental stereo-dynamical effect. In this case, the O_2 (0, 1) molecule impinges on the surface with a *cartwheel*-type motion. For a useful comparison, Fig. 6 shows an example of trajectory (1D and 3D) for O_2 (0, 1) molecule colliding at the same E_{coll}, but with a *helicopter*-type motion.

Looking at Fig. 5a panel α and Fig. 5b, we observe that up to the first bounce on the surface, the rotational motion of O_2 (0, 1) is of *cartwheel*-type. From an energy point of view, after this first jump, the translational energy of both atoms in the molecule (panel χ) decreases (both atoms decelerate) and simultaneously the rotation state, defined by j(t) (panel β), jumps to a value higher than $j = 20$. Then, this impact causes an excitation and a trapping of the molecule that continues to move close to the surface maintaining an excited rotational motion of *cartwheel* type. In particular, j(t) remains constant as well as, on average, the translational energy (E_{tr}) of the molecule, because the E_{tr} component of one of two atoms increases and that of the other decreases (panel (χ). At about t = 1500 fs, that is when an atom in the molecule (red line) comes close to the surface, j(t) undergoes another little increase. However, within a few tens of fs, the molecular rotation undergoes a decrease in conjunction with the approach of the other atom (blue line) to the surface. This sequence of events repeats again for some time before the molecule acquires internal energy sufficient to leave the surface and to go in the gas phase. In the case here examined this passage occurs with a strong decrement of rotational number. The assumed j_f is significantly larger than $j_i = 1$. Panels (δ) of Fig. 5a show the time evolution of energy transferred to the surface.

On the other hand, Fig. 6 suggests that a molecule, impinging on the surface at the same E_{coll} of trajectory in

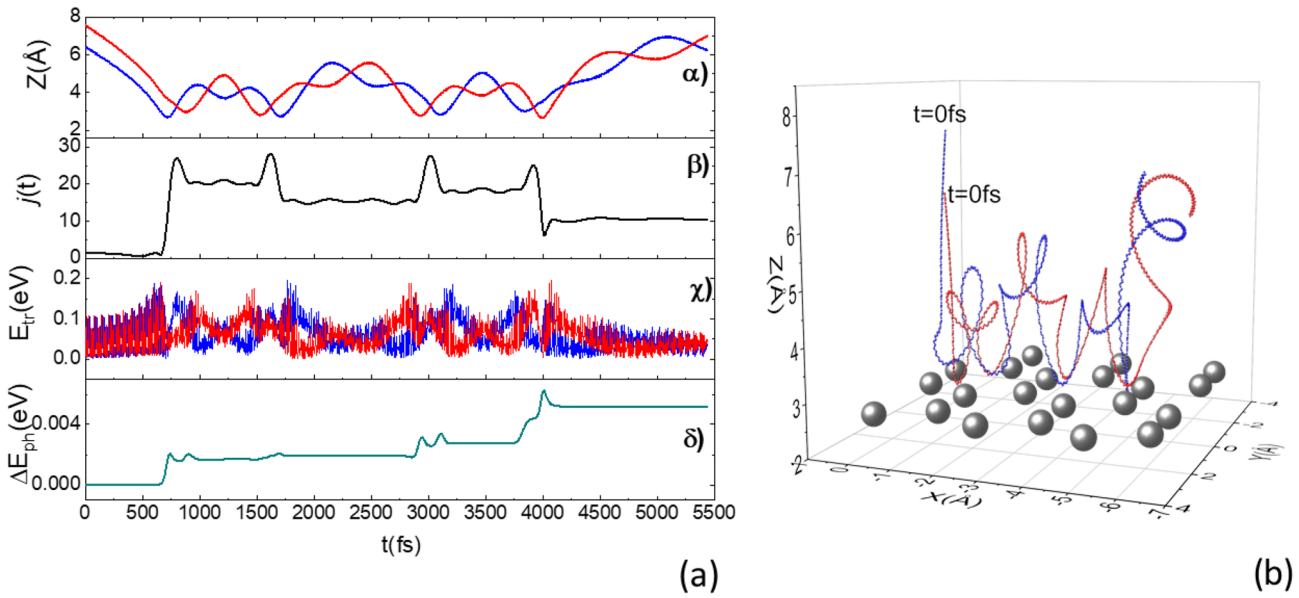

Fig. 5 (Partially adapted from Fig. 3 of Rutigliano and Pirani 2020b) Trajectory for O_2 (0, 1) at $E_{coll}=0.1$ eV backscattered in gas phase as O_2 (0, 11). The behaviour of two oxygen atoms is represented as blue and red lines. **a** Panel (α): dependence on the time t of *Z*, the normal coordinate, for the two atoms in the O_2 molecule; **a** panel (β): rotational state evolution along the trajectory; **a** panel (χ): kinetic energy of the two O atoms in the molecule; **a** panel (δ): energy exchanged with the surface phonons along the trajectory; **b** 3D trajectory in which the cartwheel-type motion is depicted. The C atoms on the surface first layer (an up-shift has been made from their position $Z=0$) are also reported (dark grey spheres)

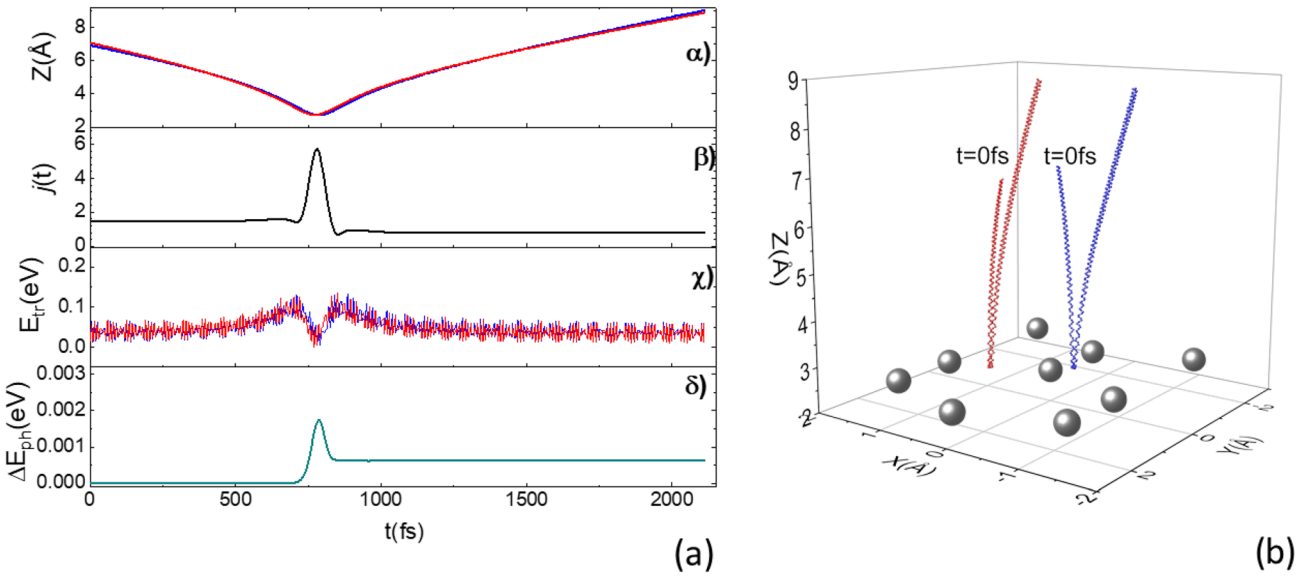

Fig. 6 (Partially adapted from Fig. 4 of Rutigliano and Pirani 2020b) Trajectory for O_2(0, 1) at $E_{coll}=0.1$ eV backscattered in the gas phase in O_2(0, 1). **a** The physical quantities shown in the panels are the same as in Fig. 5a); **b** 3D trajectory in which the *helicopter*-type motion is depicted. The C atoms on the surface first layer (an up-shift has been made from their position $Z=0$) are also reported (dark grey spheres)

Fig. 5, but moving with a *helicopter*-type motion, does not change or changes slightly its rotational number and is scattered by a direct mechanism. In this case when both atoms come close to the surface ($t \approx 750$ fs), a decrement of kinetic energy [Fig. 6 panel (χ)] of both atoms occurs with a simultaneous small increment of the rotational number [Fig. 6 panel (β)] and with a small fraction of the energy transferred to the surface [Fig. 6 panel (δ)].

Therefore, it can be useful to emphasize (see also Rutigliano and Pirani 2019) that the microscopic mechanisms determining observed stereo-dynamical effects can be related to some conjectures introduced to rationalize the molecular alignment in seeded supersonic MB (Aquilanti et al. 1999). This finding arises from the fact that the mechanisms of both phenomena, must be complementary for the following reasons: (1) the rotational relaxation in gaseous expansions occurs at low collision energies, when rotational excitations are not very probable, while the O_2 molecule excitation at graphite surface starts to become evident at intermediate E_{coll}; (2) several carrier gas-seeded molecule collisions, promoting many rotational jumps, each one with small changes in j, are necessary to observe the phenomenon in MB because the anisotropic intermolecular forces at play are weak and then less efficient, and collisions can occur with different impact parameters. In molecule–surface scattering, the selectivity is favoured by the stronger anisotropic interaction and by the higher collision energies involved. However, both in the MB alignment and in the scattering by surface, it is found that *cartwheel* molecules show the highest propensity to give rotation inelastic events.

4.3 Nitrogen

The interaction of N_2 with a graphite surface exhibits a behavior analogue to that described in the previous subsection for the O_2. Some limited differences exist that substantially should be attributed to a different coupling between the rotational and translational motion that is controlled by physisorption and/or stimulated by the coupling with the motion of the phonons of the surface. Note that the PES for nitrogen is very akin to that assumed for oxygen molecules interaction, suggesting that most of the differences with respect to O_2 are stimulated by the different molecular motion-surface phonons coupling. Moreover, the selectivity with regard to the excitation/de-excitation of rotational levels, controlled by the initial orientation of the molecular rotation axis (or rotation plane) with respect to the surface, is observed only for low collision energies while is lost under thermal and hyper-thermal collision energy conditions.

As in the case of oxygen, also for nitrogen the molecule impacting on the surface can interact through a direct or indirect mechanism. In the first case, it is immediately re-emitted in the gas phase, while in the second case, it remains trapped on the surface and moves on the surface by rebounds and at the end, it can be scattered or remain adsorbed. But, unlike the oxygen case, the interaction dynamics appears governed by E_{coll} and j_i values. In particular, the 0.1 eV collision energy represents a watershed for low j_i, so that in the dynamics it is possible to distinguish four different regimes: (i) low collisional energies and low j_i; (ii) $E_{coll} = 0.1$ eV and low j_i; (iii) $E_{coll} > 0.1$ eV and low j_i; (iv) high j_i. This can be inferred by looking at Fig. 7, where the probability for single and multiple bounces is reported for the lowest collision energy considered in this investigation and for $E_{coll} = 0.1$ eV. It appears that, while for the collision regime (i), the interaction occurs only through multiple bounces, for the highest E_{coll} value the direct (single bounce) mechanism becomes more likely as j_i increases, fixed v_i.

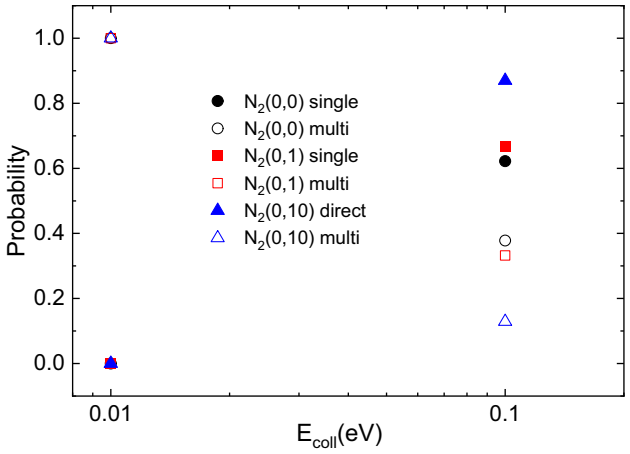

Fig. 7 Probability for single and multi-bounce in the scattering of $N_2(v_i; j_i)$ at $E_{coll} = 0.01$ eV and $E_{coll} = 0.1$ eV. Note that at $E_{coll} = 0.01$ eV the scattering occurs exclusively via the multi-bounce mechanism

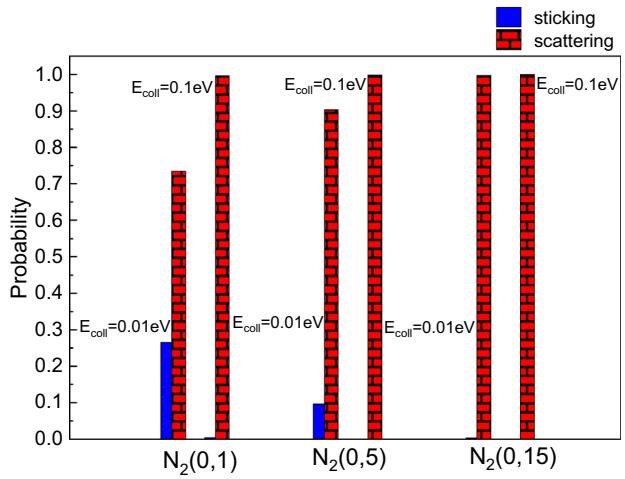

Fig. 8 As in Fig. 4 but for nitrogen molecule

The occurrence of multi-bounce in the case of nitrogen interaction reduces the probability of sticking compared to the case of the oxygen molecule, as can be deduced by looking at the data shown in Fig. 8 for nitrogen.

A peculiarity observed for nitrogen molecule, mainly for the regime (i), closely related to the exchange with surface phonons, is the synchronization–desynchronization

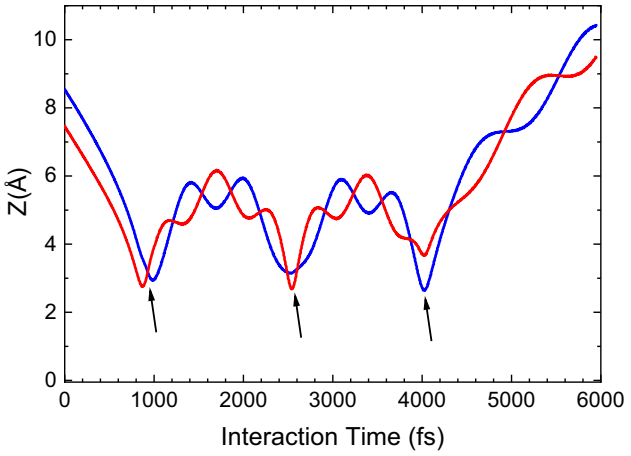

Fig. 9 Z component of the trajectory, followed by the two nitrogen atoms in the $N_2(0, 1)$ molecule impinging on graphite with $E_{coll} = 0.1$. The arrows indicate the time at which the desynchronization occurs. $T_S = 100$ K

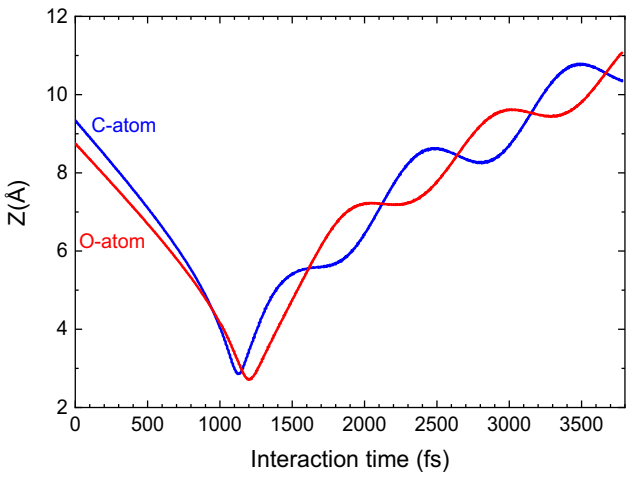

Fig. 10 Z component of the trajectory followed by C and O atoms in the CO (0; 0) approaching the surface with $E_{coll} = 0.1$ eV. $T_S = 100$ K

in the relative movement of the two N atoms, while the molecule bounces close to the surface, with a well-defined internal motion type (*helicopter/cartwheel*) with respect to the surface (Rutigliano and Pirani 2020a). This effect can be easily inferred in Fig. 9 where the Z-coordinate in the assumed reference frame for the two atoms in the N_2 molecule is reported as a function of interaction time.

The synchronization–desynchronization in the relative movement of the two N atoms, not observed in the case of the oxygen molecule, can be ascribed to the interaction with the surface phonons. In fact, as argued in (Rutigliano and Pirani 2020a), the frequency corresponding to the minimum of interaction potential on the different sites and for different molecular orientations corresponds to a zone of relative minimum in the spectrum of phonon states. Conversely, for an oxygen molecule, this frequency is located in a region of relative maximum and therefore several phonon states can participate in the interaction, allowing the motion of both atoms in the molecule to be sustained.

This has been lately confirmed also for nitrogen interaction with a tungsten surface (Rutigliano and Pirani 2023).

4.4 Carbon monoxide

The heteronuclear character of carbon monoxide molecule brings out a new intriguing stereodynamic effect on inelastic scattering, through both single-/multi- rebound mechanisms. For collision energy lower than the thermal one, it emerges a propensity to the scattering for molecules approaching with O-end closer and facing the surface. The initial vibrational state is preserved and also for this interaction we observe the selectivity with regard to the excitation/de-excitation of rotational levels controlled by the initial orientation of the molecular rotation axis.

In addition to these peculiarities, the heteronuclear nature of the carbon monoxide molecule and the resulting different attraction/repulsion of the C-end compared to the O-end give rise to new stereodynamic effects, observable especially at low collision energy, when the collision times become sufficiently long allowing for molecular reorientation effects. In fact, molecule C-end bends towards the surface while approaching this latter, due to the anisotropic physisorption attraction. This appears in Fig. 10 where a trajectory for a molecule, initially approaching with O-end towards the surface for which the C-end is folded ($t \sim 900$ fs) and reaches the minimum distance from the surface before the O-end, is displayed. Such a *steering effect* is expected to also affect the formation of CO pre-covered state on metallic surfaces of interest for heterogeneous chemical oxidation reactions (Gerbi et al. 2006).

The heteronuclear character produces also final rotational distributions in which peaks in the low j_f values are due to the molecules impinging with the O-end closer to the surface, while tails are primarily attributable to molecules approaching with the C-end towards the surface (Rutigliano and Pirani 2021). This effect is not appreciable at lower energies but becomes increasingly evident as the collisional energy increases.

5 Conclusions

The long-range interactions of gaseous species with a graphite surface have been characterized in detail leading to the analytical expression relating the dispersion attraction

coefficient C_3 with the polarizability of any impinging species. Similar results have been recently obtained for systems involving a W(100) surface for which an important test, concerning the comparison between prediction and measurement of the sticking coefficient of N_2 molecule, has been possible (Rutigliano and Pirani 2023).

In addition, the ILJ potential model has been used to formulate and study the role of the interaction potential, operating at intermediate and large separation distances and controlling the collision dynamics of diatomic molecules, such as H_2, O_2, N_2, and CO, with a graphite surface. The methodology, adopted for the description of the interaction of diatomic molecules with a graphite surface, has been proper to characterize relevant features of the inelastic collisions for E_{coll} values ranging from sub-thermal to thermal conditions. This choice emphasizes the role of the long-range forces, specifically their strength, range and anisotropy. Moreover, also the coupling with the surface phonons, mainly enhanced for low collision energies, clearly emerges. MD simulations, through propagation and analysis of thousands of trajectories, have been then crucial to characterize some basic features of the scattering process and its products, in the past highlighted and studied for metallic surfaces.

Therefore, it can be stressed that the molecule–surface scattering, driven by anisotropic force fields, can be an important tool to emphasize relevant stereodynamics effects controlling a myriad of elementary processes of general interest and occurring at the gas–surface inter-phases.

Funding Open access funding provided by Consiglio Nazionale Delle Ricerche (CNR) within the CRUI-CARE Agreement.

Data Availability The authors declare that the data supporting the findings of this study are available on request.

References

Agúndez M, Wakelam V (2013) Chemistry of dark clouds: databases, networks, and models. Chem Rev 113:8710–8737. https://doi.org/10.1021/cr4001176

Ambrosetti A, Silvestrelli PL (2012) Phys Rev B 85:073101. https://doi.org/10.1103/PhysRevB.85.073101

Aquilanti V, Ascenzi D, de Castro-Vitores M, Pirani F, Cappelletti D (1999) A quantum mechanical view of molecular alignment and cooling in seeded supersonic expansions. J Chem Phys 111:2620–2632. https://doi.org/10.1063/1.479537

Billing GD (2000) Dynamics of molecule surface interactions. Wiley, New York

Cacciatore M, Rutigliano M (2009) Dynamics of plasma–surface processes: E-R and L–H atom recombination reactions. Plasma Sources Sci Technol 18:023002. https://doi.org/10.1088/0963-0252/18/2/023002

Cambi R, Cappelletti D, Liuti G, Pirani F (1991) Generalized correlations in terms of polarizability for van der Waals interaction potential parameter calculations. J Chem Phys 95:1852–1861. https://doi.org/10.1063/1.461035

Cartry G, Schiesko L, Hopf C, Ahmad A, Carrère M, Layet JM, Kumar P, Engeln R (2012) Production of negative ions on graphite surface in H_2/D_2 plasmas: experiments and SRIM calculations. Phys Plasmas 19:063503. https://doi.org/10.1063/1.4725188

Casolo S, Tantardini GF, Martinazzo R (2013) Insights into H_2 formation in space from ab intio molecular dynamics. PNAS. https://doi.org/10.1073/pnas.1301433110

Creighan SC, Perry JSA, Price SD (2006) The rovibrational distribution of H2 and HD formed on a graphite surface at 15–50 K. J Chem Phys 124:114701. https://doi.org/10.1063/1.2174878

Gerbi A, Savio L, Vattuone L, Pirani F, Cappelletti D, Rocca M (2006) Role of rotational alignment in dissociative chemisorption and oxidation: O2 on bare and CO-precovered Pd(100). Angew Chem Int Ed 45:6655–6658. https://doi.org/10.1002/anie.200602180

Hanna AR, Van Surksum TL, Fisher ER (2019) Investigating the impact of catalysts on N_2 rotational and vibrational temperatures in low pressure plasmas. J Phys D: Appl Phys 52:345202

Israelachvili JN (1991) Intermolecular & surface forces. Academic Press, p 156

Kristensen LE, Amiaud L, Fillion J-H, Dulieu F, Lemaire J-H (2011) H_2, HD, and D_2 abundances on ice-covered dust grains in dark clouds. Astron Astrophys 527:A4. https://doi.org/10.1051/0004-6361/200912124

Lea LR, Winter R, Chen JG (2020) N_2 fixation by plasma-activated processes. Joule 5:300–315. https://doi.org/10.1016/j.joule.2020.11.009

Olney TN, Can NM, Cooper G, Brion CE (1997) Absolute scale determination for photoabsorption spectra and the calculation of molecular properties using dipole sum-rules. Chem Phys 223:59–98. https://doi.org/10.1016/S0301-0104(97)00145-6

Pirani F, Brizi S, Roncaratti LF, Casavecchia P, Cappelletti D, Vecchiocattivi F (2008) Beyond the Lennard–Jones model: a simple and accurate potential function probed by high resolution scattering data useful for molecular dynamics simulations. Phys Chem Chem Phys 10:5489–5503. https://doi.org/10.1039/B808524B

Rutigliano M, Cacciatore M (2008) Isotope and surface temperature effects for hydrogen recombination on a graphite surface. ChemPhysChem 9:171–181. https://doi.org/10.1002/cphc.200700394

Rutigliano M, Pirani F (2016) Selectivity in the inelastic rotational scattering of hydrogen molecules. Chem Phys 479:11–19. https://doi.org/10.1016/j.chemphys.2016.09.002

Rutigliano M, Pirani F (2018) Selectivity in the inelastic rotational scattering of D_2 and HD molecules from graphite: similarities and differences respect to the H_2 case. Chem Phys 504:38–47. https://doi.org/10.1016/j.chemphys.2018.02.024

Rutigliano M, Pirani F (2019) On the influence of rotational motion of oxygen molecules on the scattering from graphite surfaces. J Phys Chem C123:11752–11762. https://doi.org/10.1021/acs.jpcc.9b01966

Rutigliano M, Pirani F (2020a) Selectivity and stereodynamics effects in the scattering of nitrogen molecules from a graphite surface. J Phys Chem C124:10470–10482. https://doi.org/10.1021/acs.jpcc.0c00216

Rutigliano M, Pirani F (2020b) Rotational inelastic scattering of $H_2$and O_2molecules from graphite. Rendiconti Accademia Nazionale Delle Scienze Detta Dei XL Memorie e Rendiconti Di Chimica, Fisica, Matematica e Scienze Naturali I:69–74

Rutigliano M, Pirani F (2021) Stereodynamic effects of CO molecules scattered from a graphite surface. J Phys Chem C125:9074–9084. https://doi.org/10.1021/acs.jpcc.1c00555

Rutigliano M, Pirani F (2022) Scattering of N_2 molecules from silica surfaces: effect of polymorph and surface temperature. Molecules 27:7445. https://doi.org/10.3390/molecules27217445

Rutigliano M, Pirani F (2023) The sticking of N_2 on W(100) surface: an improvement in the description of the adsorption dynamics further reconciling theory and experiment. Molecules 28:7546. https://doi.org/10.3390/molecules28227546

Rutigliano M, Cacciatore M, Billing GD (2001) Hydrogen atom recombination on graphite at 10 K via the Eley–Rideal mechanism. Chem Phys Lett 340:13–20. https://doi.org/10.1016/S0009-2614(01)00366-9

Vattuone L, Savio L, Pirani F, Cappelletti D, Okada M, Rocca M (2010) Interaction of rotationally aligned and of oriented molecules in gas phase and at surfaces. Prog Surf Sci 85:92–160. https://doi.org/10.1016/j.progsurf.2009.12.001

Vidali G, Ihm G, Kim H-Y, Cole MW (1991) Potentials of physical adsorption. Surf Sci Rep 12:133–181. https://doi.org/10.1016/0167-5729(91)90012-M

Wakelam V, Bron E, Cazaux S, Dulieu F, Gry C, Guillard P, Habart E, Hornekær L, Morisset S, Nyman G, Pirronello V, Price SD, Valdivia V, Vidali G, Watanabe N (2017) H_2 formation on interstellar dust grains: the viewpoints of theory, experiments, models and observations. Mol Astrophys 9:1–36. https://doi.org/10.1016/j.molap.2017.11.001

Werner H-J, Meyer W (1976) Finite perturbation calculations for the static dipole polarizabilities of the first-row atoms. Phys Rev A 13:13–16. https://doi.org/10.1103/PhysRevA.13.13